Buzdin, Shapiro, and chimera steps in φ_0 Josephson junctions. II. Bifurcation, switching, and hysteresis

M. Nashaat [1,2,*] E. Kovalenko [3] and Yu. M. Shukrinov [1,4,5,†]
[1]*BLTP, JINR, Dubna, Moscow region 141980, Russia*
[2]*Department of Physics, Faculty of Science, Cairo University, 12613 Giza, Egypt*
[3]*Center for the Development of Digital Technologies, Krasnogorsk 143407, Russia*
[4]*Dubna State University, Dubna, Moscow region 141980, Russia*
[5]*Moscow Institute of Physics and Technology, Dolgoprudny 141700, Russia*

(Received 20 March 2024; revised 28 May 2024; accepted 26 June 2024; published 18 July 2024)

The dynamics of magnetization and current-voltage characteristics of the superconductor-ferromagnet-superconductor φ_0 Josephson junction in the presence of external electromagnetic radiation have been studied. Effects of the electric and magnetic components of radiation on the magnetic precession in the ferromagnetic layer are investigated. The implementation of two types of dynamical states of magnetization is demonstrated. These states have a phase shift of π in the synchronization region of magnetic precession and Josephson oscillations and differ in the nature of their time dependence. Transitions between these states with increasing and decreasing bias current show hysteresis, which is reflected in the bifurcation diagram and as spikes in the current-voltage characteristics. We also provide an experimental way to test the obtained results by measuring the phase shift in voltage temporal dependence at fixed current value for both sweeping directions. The results obtained can find application in various fields of superconducting spintronics and quantum computing.

DOI: 10.1103/PhysRevB.110.024510

I. INTRODUCTION

The coexistence and mutual influence of superconductivity and magnetism is one of the most pressing problems in condensed matter physics [1–6]. An important achievement in this area is the implementation of the coupling between the superconducting phase and magnetic moment in superconductor-ferromagnet-superconductor Josephson junctions (JJ) with strong spin-orbit coupling [7,8]. A series of interesting results in this field describing anomalous or φ_0 junctions with the phase shift in the ground state and the Josephson junctions on topological insulators are obtained recently [3,7,9–14].

Experimentally, it is easier to break the time-reversal symmetry by a magnetic field applied to the Josephson junction. In this case, the junction has a phase shift caused by the Zeeman effect [15–18]. However, it is very attractive to realize the anomalous φ_0 junction in the structures with ferromagnetic layer, and open up the possibilities for magnetization control and its applications in such structures [19–23]. This leads to a number of different directions in superconducting spintronics, based on reversing the magnetic moment of the ferromagnetic layer [24,25], phase batteries [26], diode effect [27,28], cryogenic spintronics devices [22,29]. Interesting perspectives are opened by applications based on Kapitza pendulum features demonstrated by the φ_0 junction [30], as well as the unique nonlinear phenomena [31–35].

Furthermore, ferromagnetic resonance (FMR) manifests the reach physics in the anomalous Josephson junctions. In Ref. [36], it is shown that as a current sweep along the I-V characteristics of the φ_0 junction, it leads to regular magnetization dynamics with a series of specific phase trajectories related to a direct coupling of the magnetic moment and the Josephson oscillations. The magnetization dynamics in SFS thin film structures by ferromagnetic resonance spectroscopy was investigated in Ref. [6]. The one-dimensional anisotropic action of superconducting torque on magnetization dynamics was experimentally established. The authors results support the recently proposed by M. Silaev the mechanism of the superconducting torque formation via the interplay between the superconducting imaginary conductance and magnetization precession at superconductor-ferromagnet interfaces. So, S-F-S systems provide the playground for Anderson-Higgs mass generation of boson quasiparticles in high-energy Standard Model and in condensed-matter systems [6,37].

Recently, it was demonstrated in Ref. [38], the JJ's supercurrent can be nonlocally controlled by the phase difference of another JJ. This occurs when the two JJs sharing a single superconducting electrode and are coherently connected forming the Andreev molecules. The results demonstrate that even in the case of a zero local phase difference, the nonlocal phase control produces a finite supercurrent. Strong magnetic field and ferromagnetic material are not necessary for this realization.

In Ref. [23], the authors demonstrate the possibility of controlling the magnetic states in chain of φ_0 junctions. The static and dynamic magnetic properties of such a system reveals the manifestation of an n-level system, in which the

*Contact author: majed@sci.cu.edu.eg
†Contact author: shukrinv@theor.jinr.ru

energies of the levels are determined by only projections of the total magnetic moment $\sum M_i$ onto the easy magnetic axis. Also, it is shown that the total magnetic moment can be controlled by a superconducting current. Another possibility for influencing the properties of the φ_0 junction arises under external electromagnetic radiation, leading to synchronization of Josephson oscillations and magnetic precession in the ferromagnetic layer [39].

Our previous work [40] revealed important findings after taking into account the interaction of the magnetic field of microwave radiation with the magnetic moment of the ferromagnetic layer. It leads to a number of unique resonant and synchronization phenomena, in particular, the manifestation of two mechanisms of synchronization of Josephson oscillations and magnetic precession. Due to the coupling of superconductivity and magnetism in this system, the precession of the magnetic moment of the ferromagnetic layer, caused by the magnetic component of the external radiation, can synchronize Josephson oscillations, leading to the appearance of a special type of steps in the current-voltage characteristic, completely different from the known Shapiro steps. These steps were called Buzdin steps in the case when the system is driven only by the magnetic component of radiation, and chimera (due to their different and composite mechanism of the step formation) when both electric and magnetic components are taken into account. When the Josephson or external radiation frequency approaches the ferromagnetic one, then the mutual influence of Josephson and Kittel ferromagnetic resonances occurs [40].

In this work, the sweeping of bias current and magnetization dynamics along the chimera step in the I-V characteristics of φ_0 junction in the Josephson ferromagnetic resonance region is analyzed. We show two-bubble structure in the magnetization and spikes in the I-V characteristics reflecting the corresponding transitions between magnetization bubbles. These transitions demonstrate the creation of two different magnetization states caused by bifurcations in magnetic dynamics of ferromagnetic layer. The manifestation of a novel type of hysteresis related to the transitions between these states is shown. We demonstrate also a possibility of switching between the found magnetization dynamical states by electric current pulse and propose an experimental testing of the observed phenomena. Two schemes of calculations are considered here. The first one is based on two signal model, in which the magnetic and electric components come from different sources and can be tuned separately. In the second scheme both the electric and magnetic components are related to each other and come from the same radiation signal. The obtained results about hysteresis and the appearance of the two dynamical states of $m_y(t)$ can be achieved in the two schemes.

The paper is organized as follows. The model and methods are introduced in Sec. II. In Sec. III, we demonstrate the bifurcation between magnetization dynamical states and discuss the origin and specific features of two states of magnetization along the chimera step. The switching of states by current pulse along the chimera step for decreasing and increasing bias current are demonstrated in Sec. IV. In Sec. V, we discuss the hysteretic behavior of magnetization along the steps and its variation by spin-orbit coupling and radiation parameters.

FIG. 1. Schematic diagram depicting φ_0 under the influence of external electromagnetic radiation. The magnetic field component (H_R), and the anisotropic field (H_{an}) are in z direction, while the bias current I is along the x direction.

Results of the one-signal model are presented in Sec. VI. The π phase shift in supercurrent and voltage dynamics along the chimera step and possible application of the obtained results are discussed in Sec. VII. Finally, we come to the conclusions.

II. MODEL AND METHODS

In the proposed φ_0 JJ, the easy axis of the ferromagnet and the gradient of the spin-orbit potential are directed along the same axis z (see Fig. 1). In this case, the phase shift is proportional to the y component of the magnetic moment of the ferromagnet $\varphi_0 = rM_y/M_0$, where r characterizes the magnitude of the spin-orbit interaction [8], $M_0 = ||\mathbf{M}||$ is the saturation magnetization. The junction is under a linearly polarized electromagnetic radiation, which magnetic component $\mathbf{H}_R$ is also parallel to the z axis.

Dynamics of the magnetic moment is determined by the Landau-Lifshitz-Gilbert (LLG) equation [41]:

$$\frac{d\mathbf{M}}{dt} = -\gamma \mathbf{M} \times \mathbf{H}_{\text{eff}} + \frac{\alpha}{M_0}\left(\mathbf{M} \times \frac{d\mathbf{M}}{dt}\right), \tag{1}$$

where γ is the gyromagnetic ratio, α is the Gilbert damping constant. The effective field is given by [40]

$$\mathbf{H}_{\text{eff}} = \frac{K}{M_0} Gr \sin\left(\varphi - r\frac{M_y}{M_0}\right)\hat{\mathbf{y}} + \left(\frac{K}{M_0}\frac{M_z}{M_0} + H_R \sin(\Omega_R t)\right)\hat{\mathbf{z}}, \tag{2}$$

where $G = E_J/(K\mathcal{V})$ is the ratio of the Josephson energy to the magnetic anisotropy energy, φ is the phase difference between the superconducting edges of the junction. The effective field includes the interaction between the magnetic moment of a ferromagnet and the magnetic field of external radiation

$$W_R = -\mathbf{M} \cdot \mathbf{H}_R, \tag{3}$$

where H_R is the amplitude of the magnetic component of radiation $\mathbf{H}_R = (0, 0, H_R \sin(\Omega_R t))$, Ω_R is the radiation frequency.

To describe the coupled dynamics of the magnetization and the superconducting phase difference, we solve the LLG equation together with the RCSJ equation. In this study, we consider a case of the current biased JJ, where the external current I flows through the system according to the extended RCSJ model [42]. In our calculations, we change the current direction, decreasing and increasing it in some intervals of interest. The total system of equations in the dimensionless

form that describes the magnetic and phase dynamics for φ_0 JJ is given by [40]

$$\begin{aligned}
\dot{m}_x &= \frac{1}{\alpha^2+1}\{\omega_F[-m_y m_z + Grm_z\sin(\varphi - rm_y) \\
&\quad - \alpha(m_x m_z^2 + Grm_x m_y \sin(\varphi - rm_y))] \\
&\quad - h_R(\alpha m_x m_z + m_y)sin(\omega_R t)\}, \\
\dot{m}_y &= \frac{1}{\alpha^2+1}\{\omega_F[m_x m_z \\
&\quad - \alpha(m_y m_z^2 - Gr(m_x^2 + m_z^2)sin(\varphi - rm_y))] \\
&\quad - h_R(\alpha m_y m_z - m_x)sin(\omega_R t)\}, \\
\dot{m}_z &= \frac{1}{\alpha^2+1}\{\omega_F[-Grm_x sin(\varphi - rm_y) \\
&\quad - \alpha(Grm_y m_z sin(\varphi - rm_y) - m_z(m_x^2 + m_y^2))] \\
&\quad + h_R\alpha(m_x^2 + m_y^2)sin(\omega_R t)\}, \\
\dot{V} &= [I + A\sin(\omega_R t) - V(t) + r\dot{m}_y - \sin(\varphi - rm_y)]/\beta_c, \\
\dot{\varphi} &= V(t), \qquad (4)
\end{aligned}$$

where $m_i = \frac{M_i}{M_0}(i \equiv x, y, z)$, and $\beta_c = 2eI_cCR^2/\hbar$ is the McCumber parameter. Here, the time is normalized in units ω_c^{-1}, where $\omega_c = 2eI_cR/\hbar$ is a characteristic frequency of the junction. The ferromagnetic resonance frequency $\Omega_F = K\gamma/M_0$, the frequency of external radiation, and the amplitude of magnetic component $\mathbf{H_R} = (0, 0, h_R\sin(\Omega_R t)$ are normalized to ω_c, so that $\omega_F = \frac{\Omega_F}{\omega_c}$, $\omega_R = \frac{\Omega_R}{\omega_c}$, and $h_R = \frac{\gamma}{\omega_c}H_R$. A is the amplitude of the current caused by the electric component of external radiation, and it is normalized to I_c; the external current I is also expressed in units of I_c, and the voltage V in units of $V_c = I_cR$. So, the Josephson frequency $\omega_J = V$, where V denotes the time average of the instantaneous voltage $V(t)$. The last term in the current equation (4) was derived in the framework of microscopic theory for anomalous Josephson junction in Ref. [20]. In our simulations, if it is not mentioned, we use the following model parameters: $G = 0.01$, $\alpha = 0.01$, $\beta_c = 25$, $\omega_F = 0.5$, and $r = 0.4$.

III. TWO DYNAMICAL STATES OF MAGNETIZATION ALONG THE CHIMERA STEP

As it was demonstrated in Ref. [40], the magnetization precession is changing along the Buzdin and chimera steps, though the Josephson oscillations are locked to the external electromagnetic radiation. The $m_y^{\max}(I)$ dependence demonstrates the specific "bubble like" feature in the current interval corresponded to the step. Here we show that the variation of φ_0 junction parameters, in particular, increasing the spin-orbit interactions, or changing direction of bias current, shows more complex behavior. The I-V characteristics along the Buzdin and chimera steps demonstrate the spikes related to the transitions between different dependencies of $m_y^{\max}(I)$ with increasing and decreasing the bias current.

Let us first examine the bifurcation $m_y^{\mathrm{BF}}(I)$ and average of $m_y^{\mathrm{av}}(I)$ along the chimera step. To realize it, we solve the system of equations (4) numerically. In Fig. 2(a), we present the results of one loop calculations (increasing bias current from 0 till 1.2 and back) for the I-V characteristics and the maximal value of $m_y^{\max}(I)$ for the φ_0 junction under external electromagnetic radiation. As we see, $m_y^{\max}(I)$ demonstrates split resonance peak in the region of $V = \omega_F = 0.5$, its subharmonic and second harmonic. The chimera step which appears at $V = \omega_R = 0.485$, has a jump (spike), which coincides in position with a specific feature in the $m_y^{\max}(I)$ dependence (see hollow arrow in the inset). The $m_y^{\max}(I)$ demonstrates the usual bubble structure along the chimera step.

The origin for this spike is clarified in Fig. 2(b) which shows together the I-V characteristics, $m_y^{\max}(I)$, the bifurca-

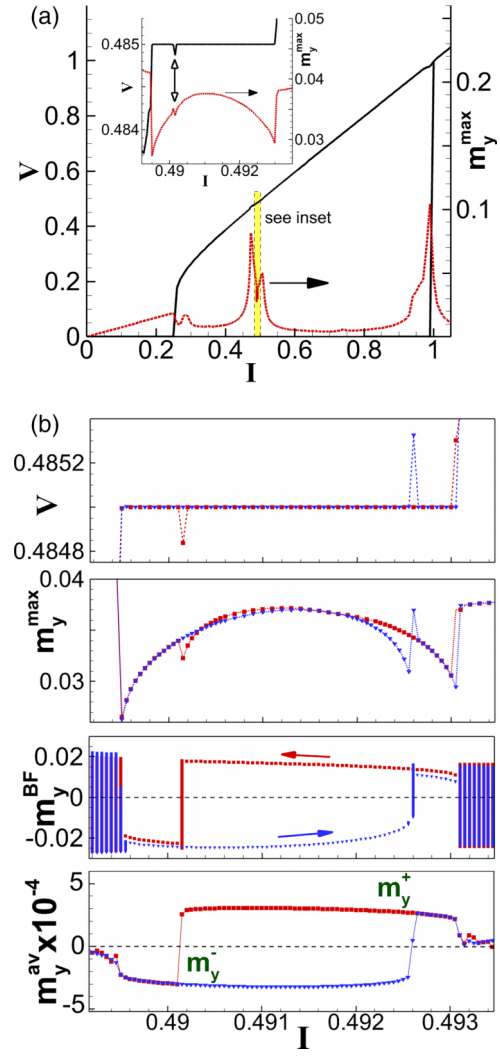

FIG. 2. (a) Manifestation of chimera step in the current-voltage characteristics and $m_y^{\max}(I)$ dependence for the φ_0 junction under external electromagnetic radiation with $A = 0.005$ and $h_R = 1$. The current region where synchronization of Josephson oscillations and precession of the magnetic moment occurs is shown in the inset. (b) Enlarged part of I-V characteristics, $m_y^{\max}(I)$, $m_y^{\mathrm{BF}}(I)$, and $m_y^{\mathrm{av}}(I)$ along the chimera step in the case of a decrease in current (red curve) and in the case of an increase of current (blue curve). All calculations are done at $r = 0.4$, $\omega_R = 0.485$. The arrows indicate the direction of bias current changing.

tion curves $m_y^{\rm BF}(I)$ for $m_y(t)$ and the averaged value $m_y^{\rm av}(I)$ in the vicinity of the chimera step for two directions in the bias current: decreasing (red) and increasing (blue). The $m_y^{\rm max}(I)$ dependence demonstrates two bubble structure: one bubble appears in the decreasing the bias current, another one in the increasing current. The bifurcation diagram calculations supports this conclusion. It is constructed by mapping for each current value a set of values m_y taken through an integer number of radiation periods: $m_y(t_0 + 2n\pi/\omega_R)$, where n is an integer. This creates the Poincaré sections at each bias current's value. For the current value outside the step, these sets form vertical columns of finite height, since in this region the magnetization dynamics is not synchronized with the external field oscillations. In the current interval, corresponding to the chimera step (synchronization region), these sets show one point on the Poincaré section indicating one period motion (*p1* motion) [43], except for the current values corresponding to transitions between the bifurcation curves with positive and negative $m_y^{\rm BF}$. Moreover, on the chimera step an interesting feature is demonstrated for $m_y^{\rm av}$, which manifests two states with positive and negative values. Depending on the sign of $m_y^{\rm av}$, we mark those states as m_y^+ for positive values of $m_y^{\rm av}(I)$, and m_y^- for negative vales of $m_y^{\rm av}(I)$. Those states are manifested on $m_y^{\rm av}(I)$ which shows also two curves with positive and negative $m_y^{\rm av}$. For each bubble, the average value could be positive or negative. At transition points, a restructuring of synchronization occurs, and we see Poincaré sections in the form of vertical segments. One transition point is in the direction of decreasing current, and the another is in the direction of increasing current. On the *I-V* characteristics, these points appear in the form of voltage spikes shown in the Fig. 2(b).

To clarify the appearance of bubble structures in the $m_y^{\rm max}(I)$ dependence and the occurrence of magnetization bifurcations, we studied the time dependence of m_y at the bifurcation points. This dependence at a current value of $I = 0.49005$, where magnetization bifurcation occurs as the current decreases, is presented in Fig. 3(a).

We observe a change in the nature of the m_y dynamics during the transition process. Before the transition, the oscillations of $m_y(t)$ occur predominantly in the region of positive values of m_y, and after, mainly in the region of negative values, corresponding to the dynamical states of magnetization m_y^+ and m_y^-, respectively. This fact is also demonstrated by the moving average value which is denoted by m_y^{mav}. Instead of arithmetic average (which static in time), the moving average is the mean of a time series for a specified period, it is continually recalculated based on the latest point value. In Fig. 3(a), it is shown in black line, reflecting the states of m_y^+ before the bifurcation and m_y^- after that. The averaging period when calculating m_y^{mav} was chosen equal to the period of external radiation. Oscillations in the intervals highlighted in blue and green are shown in an enlarged scale in the Figs. 3(b) and 3(c), respectively. We note that at such transition, a phase difference shift of π occurs in the time dependence of voltage and superconducting current.

The nature of the change in the dynamics of m_y is also clarified by Figs. 3(d) and 3(e), which show magnetization trajectories in the $m_x - m_y$ plane in the states m_y^+ and m_y^-, respectively. The characteristic curl of the motion trajectory

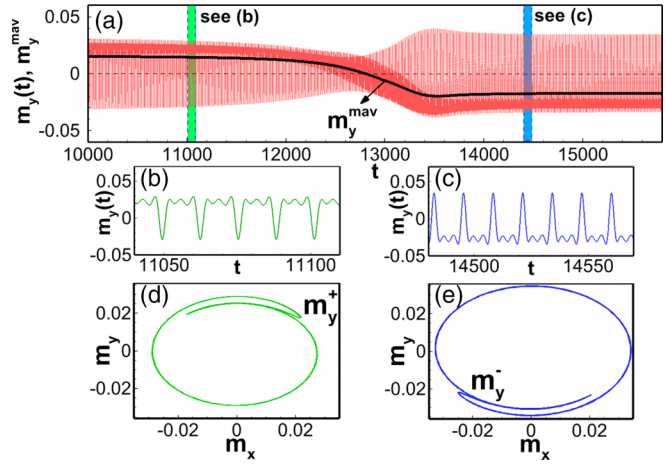

FIG. 3. The change in the m_y component dynamics in the case of the transition $m_y^+ \to m_y^-$ at $I = 0.49005$ (with decreasing current). (a) The corresponding time dependence in the transition region, (b) and (c) represent the enlarged parts of m_y time dependence before the transition (state m_y^+) and after (state m_y^-), and (d) and (e) show the corresponding magnetization trajectories in the plane $m_x - m_y$.

(usually called the "mother-in-law's tongue") for the state m_y^+ is in the region of positive values of m_y, and in the region of negative values for the state m_y^-. It is important to note that these transitions appear on the *I-V* characteristics in the form of spikes and, therefore, can be detected experimentally. It becomes possible to control the synchronization of magnetization in the φ_0 junction and change its state along the *I-V* curve.

It would be interesting to compare the observed results for chimera step with the corresponded results for the Shapiro and Buzdin steps. In Fig. 4(a), we present an enlarged part of the *I-V* characteristics with Shapiro step ($h_R = 0$). As we see, for the Shapiro step $m_y^{\rm max}(I)$ values has a very small variation, almost constant, along the step (see inset). The average value of $m_y(t) \approx 10^{-6}$ along the Shapiro step is almost zero. In addition to this, the curves along the Shapiro step for the current simulation parameters coincide for both direction of current (decreasing and increasing), i.e., two bubble structure does not appear, and thus the two states $m_y^{\pm}(I)$ are not manifested.

The results for the Buzdin step are presented in Fig. 4(b). Similar to chimera, the Buzdin step ($A = 0$) demonstrates two bubble structure for $m_y^{\rm max}(I)$ with the decreasing and increasing current. The intersection between the bubbles is manifested by spike on the Buzdin step in the *I-V* characteristics at $I = 0.4899$ for decreasing current and at $I = 0.4925$ for increasing current (see Ref. [44]). Also, $m_y^{\rm av}(I)$ shows non-symmetrical hysteresis [see dashed horizontal line in Fig. 4(b)]. As we mentioned above, this feature opens the way for experimental testing of the observed steps. We stress that in difference with chimera and Buzdin steps, the variation in $m_y^{\rm max(min)}(t)$ values along the Shapiro step is much smaller than in the cases of Buzdin and chimera steps, with the average value $m_y^{\rm av}(I)$ almost zero. Also, the dynamic characters and results of fast Fourier transformation (FFT) for $m_y(t)$ along the Shapiro step is different from the case of Buzdin step (see Ref. [44]).

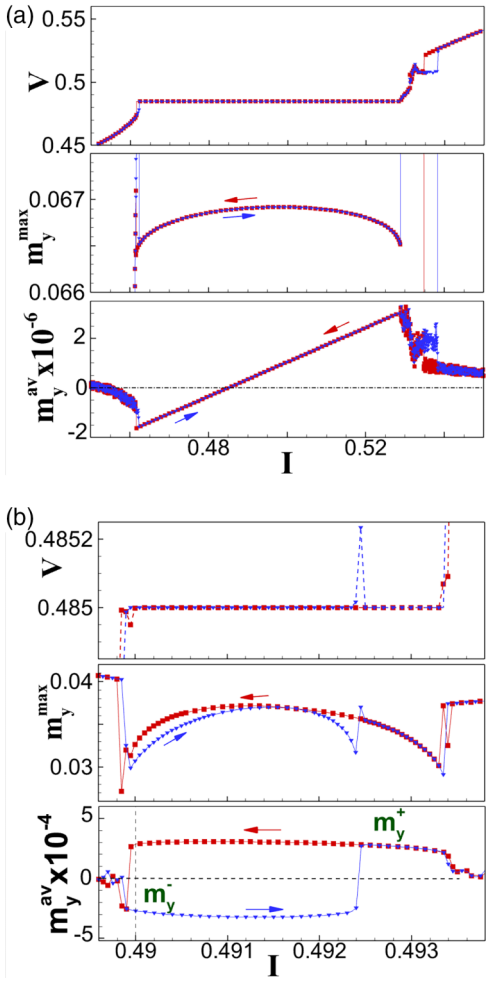

FIG. 4. Comparison of two loop calculations of I-V characteristics, $m_y^{\max}(I)$ and average of $m_y^{\mathrm{av}}(I)$ for (a) Shapiro step at $A = 0.4$ and $h_R = 0$, (b) Buzdin step at $A = 0$ and $h_R = 1$. All panels are done at $r = 0.4$, $\omega = 0.485$. The arrows indicate the direction of bias current changing.

IV. SWITCHING BETWEEN DYNAMICAL STATES

Existence of two different magnetization states m_y^+ and m_y^- in bias current interval, corresponded to the chimera or Buzdin step, creates a series of novel interesting phenomena and applications in superconducting spintronics. In particular, one of them is an implementation of controllable switching between these two states. Because the states are determined by bias current direction, one obvious way is the switching between them by sweeping or changing the current direction after the jump on the voltage step. Another way is to apply a current pulse similar to what was already discussed for magnetization reversal in the φ_0 junction [24,25]. Here we demonstrate such possibility of switching by bias current pulse of rectangular form in Fig. 5.

We have chosen an arbitrary value of bias current $I = 0.492$, at which the both two states of m_y are realized for increasing and decreasing bias current process (see Fig. 2). Switchings are demonstrated in Figs. 5(a) and 5(b) for decreasing (transition $m_y^+ \to m_y^-$) and increasing current direction ($m_y^- \to m_y^+$), respectively. With the given simulation

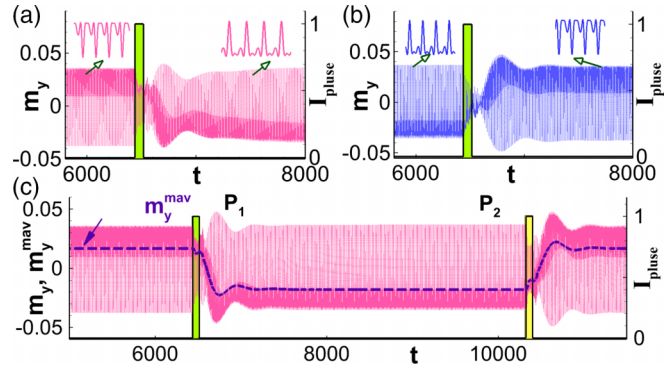

FIG. 5. Magnetization dynamics for m_y under rectangular pulse signal (a) decreasing current; (b) increasing current; (c) decreasing current with two successive pulses, the dashed line shows the moving average during these switching process. All panels are done with $r = 0.4$, $h_R = 1$, and $A = 0.005$.

parameters, the switching between the two states occurs for pulse width $6T$ and pulse amplitude $I_{\mathrm{pulse}} = 1$, where T is the period of the external electromagnetic field, and the pulse amplitude is normalized to I_c. The switching with a changed pulse parameters are shown in sections "B" of Ref. [44], demonstrated it for pulse width $8T$ and pulse amplitude $I_{\mathrm{pulse}} = 0.8$. So, the transition between states can be controlled by the pulse and model parameters, by analogy of magnetization reversal discussed in Ref. [25], Moreover, we can also control the switching between the two states in fixing the current direction and just apply successive pulses as demonstrated in Fig. 5(c), which shows the switching from m_y^+ state to m_y^- state by applying the first pulse (P_1). Then, after some time, the second pulse (P_2) switch the state m_y^- to m_y^+. The line shows a moving average during these switching process.

V. VARIATION OF HYSTERESIS BY SPIN-ORBIT COUPLING AND RADIATION PARAMETERS

Another interesting and important phenomena related to the creation of the two different magnetization states m_y^+ and m_y^- directly follows from the results, presented in Fig. 2. Sweeping current along the chimera step, decreasing it in the first loop of sweeping and increasing in the second loop, demonstrates a hysteretic behavior in the dependence $m_y^{\max}(I)$. It is also clearly pronounced in the simulations of the bifurcation $m_y^{\mathrm{BF}}(I)$ and averaged $m_y^{\mathrm{av}}(I)$ dependencies. At chosen junction and electromagnetic field parameters indicated in the caption to Fig. 2, a transition between the states $m_y^+ \to m_y^-$ (red color) occurs at $I = 0.4901$, whereas the transition $m_y^- \to m_y^+$ (blue color) happens at $I = 0.4925$, forming a hysteresis loop with width equal to $\Delta I = 0.0024$.

Figure 6 demonstrates the effect of spin-orbit interaction (SOI) on the hysteresis. It demonstrates $m_y^{\max}$ and m_y^{av} as functions of bias current at two values of SOI parameters.

As we see, at a small value of SOI parameter ($r = 0.2$), the $m_y^{\max}(I)$ curves coincide for both directions of current changing, i.e., the hysteresis is absent. The dependence $m_y^{\mathrm{av}}(I)$ manifests the both two states of $m_y^{(\pm)}$ which correspond to the right and left halves of bubble in $m_y^{\max}(I)$. As we noted in

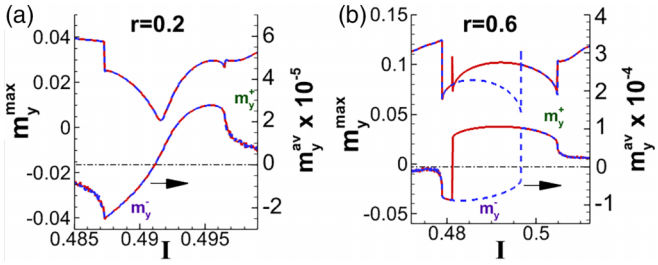

FIG. 6. Variation of the hysteresis region with a change in the spin-orbit coupling parameter. Results of two loop calculations of $m_y^{\max}(I)$ and $m_y^{\text{av}}(I)$ at (a) $r = 0.2$ and (b) 0.6.

Ref. [40], the width of Buzdin and chimera steps are growing crucially with increase in the spin-orbit coupling. Compare the results for hysteresis width ΔI at different SOI parameter, we find that it grows crucially with an increase in r as well. In particular, at $r = 0.4$, the hysteresis width $\Delta I = 0.0024$, while at $r = 0.6$, it is $\Delta I = 0.0156$. However, relatively to the step width, the hysteresis width does not change essentially.

Figure 7 shows the effect of slight variation of radiation electric component on the hysteresis features. Taking into account also results presented in Fig. 2, we can make a conclusion, that an increase in A in the interval (0.002–0.008) leads to shifting of the hysteresis region from the right part of step to the left one of the chimera step. Transition $m_y^- \to m_y^+$ with an increasing in the bias current is observed at the edge of the step. The width of the hysteresis region does not change practically. We stress ones more that the spikes in the presented I-V characteristics correspond to the transition between the two states of m_y and indicate the size of hysteresis region. The I-V characteristics of Josephson junction can be measured experimentally, so, the observing spikes in it, we indicate a direct way to investigate the transition points between two bubbles corresponded to different states of magnetization and hysteric features of the system experimentally.

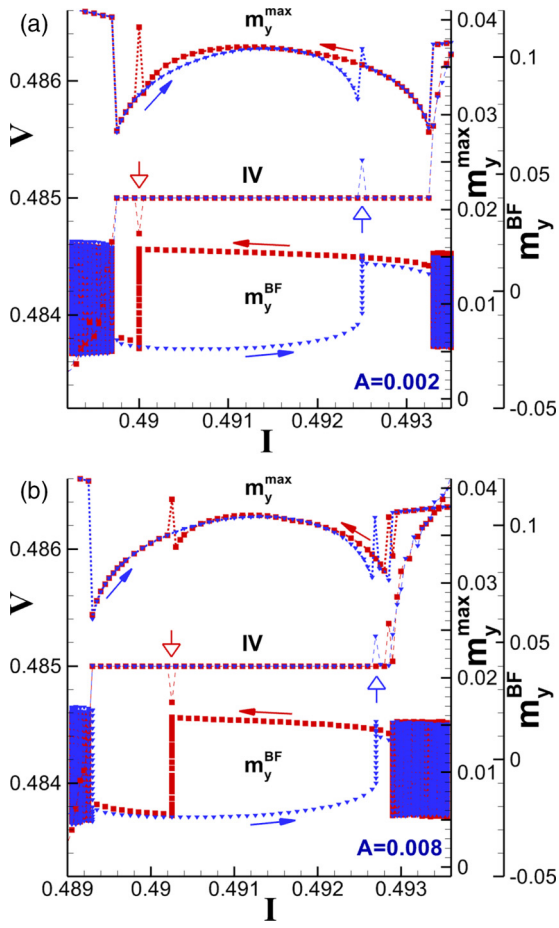

FIG. 7. Effect of external radiation on the hysteresis features. Results of two loop calculations of I-V characteristics, $m_y^{\max}(I)$ and $m_y^{\text{BF}}(I)$ at (a) $A = 0.002$ and (b) 0.008.

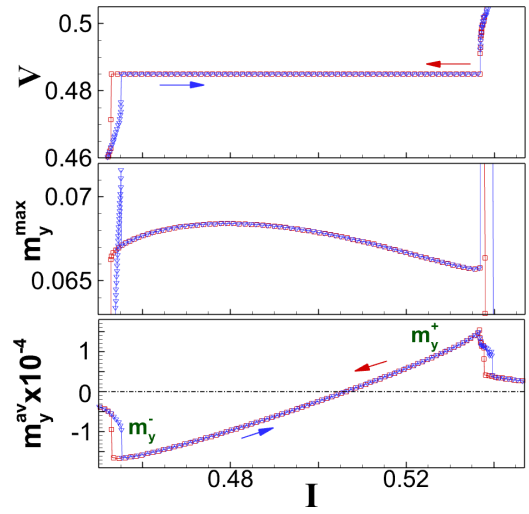

FIG. 8. An enlarged part of I-V characteristics, $m_y^{\max}(I)$, and $m_y^{\text{av}}(I)$ along the chimera step at $A = 0.5$, $h_R = 0.149$, $r = 0.4$, and $\omega_R = 0.485$.

VI. RESULTS FOR THE ONE-SIGNAL MODEL

The results of calculations in one-signal model are less expressive, but they are qualitatively consistent with the described observations. To stress this fact and prove the correctness of our conclusions, we present here two examples, demonstrating the bifurcation along the chimera step and two dynamical states of $m_y^{+(-)}$ in one-signal model. As in Ref. [40], we use the same set of model parameters: the critical current density $J_c = 10^5$ A/cm^2, the Josephson junction area (S $= 0.1 \times 0.1$) μm^2, the normal resistance $R = 1$ Ω, the characteristic frequency $\omega_c = 30$ GHz, and the relative magnetic permeability $\sim 10^5$. Using the obtained relation between h_R and A:

$$h_R = \frac{\gamma I_c A}{\nu^{3/2}\omega_c}\sqrt{\frac{2R}{S\epsilon}}, \tag{5}$$

where $\nu = 1/\sqrt{\mu\epsilon}$, considering the magnetic permeability within $10^2 \sim 10^5$, we might have the values $A = 0.5$ and h_R in the interval (0.002–0.149) for a power $P = 10^{-10}$ Watt. The power $P = 10^{-8}$ W leads to the values $A = 10$ and h_R in the interval (0.017–2.982).

As a first example, we consider the case with $A = 0.5$ and the corresponding $h_R = 0.149$. Figure 8 shows an enlarged

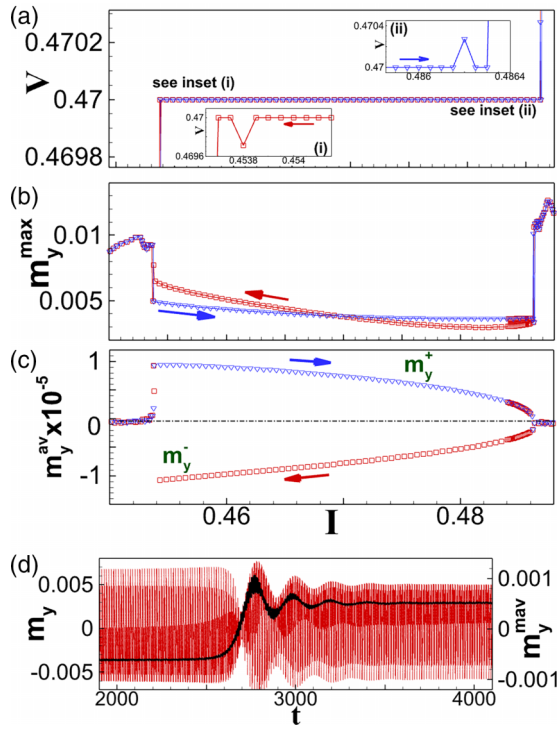

FIG. 9. (a) An enlarged part of I-V characteristics, the downward and upward insets show the voltage spike for the decreasing and increasing the bias current respectively. (b) Enlarged part of $m_y^{\max}(I)$ along the chimera step, the arrows indicate the direction of bias current changing. (c) Same as in (b) for $m_y^{\rm av}(I)$. (d) The corresponding time dependence in the transition region from $m_y^- \to m_y^+$ at $I = 0.45380$ (with decreasing current), the solid line represents the moving average. All panels are done at $A = 38.9$, $h_R = 1.64$, $r = 0.2$, and $\omega_R = 0.47$.

part of the I-V characteristics with chimera step, and the corresponding dependencies $m_y^{\max}(I)$ and $m_y^{\rm av}(I)$ for both current directions. As we see, no hysteresis is demonstrated at those values, while we have continuous transition between the two dynamical states of $m_y^{+(-)}$ by changing the current along the step.

In the second example, assuming critical current density $J_c = 10^5$ (A/cm^2), Josephson junction area (0.126×0.126) μm^2, and resistance R=1 Ω, we get the characteristic frequency $\omega_c = 48$ GHz. With microwave power $P \approx 3.8 \times 10^{-7}$ Watt, and for relative permeability 10^4, according to the relation (5), we find $h_R = 1.64$ for $A = 38.9$.

The results of calculations with these parameters are illustrated in Fig. 9. In Fig. 9(a), the I-V characteristics shows chimera step at $V = 0.47$ with two voltage spikes (see insets (i) and (ii) for the decreasing and increasing bias current respectively). The spikes appears due to the transition between the two dynamical states of m_y. The plots for $m_y^{\max}(I)$ and $m_y^{\rm av}(I)$ are shown in Figs. 9(b) and 9(c), respectively. As it can be seen, a hysteresis along the chimera step appears. Also, it can be seen that on the right side of the chimera step, where the difference between the $m^{\pm}$ states is small, an instability occurs for the maximum value $m_y^{\max}$ and the average $m_y^{\rm av}$ value fluctuates between these two states. The fluctuations disappear when the difference between the two branches become large

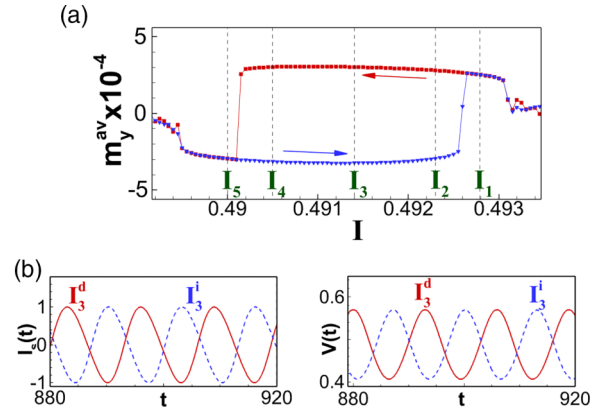

FIG. 10. Demonstration of the phase shift in the chimera step. (a) An enlarged part of the $m_y^{\rm av}(I)$ in chimera step for two loop calculations. The dashed vertical lines indicate the positions at which we have investigated the temporal dependence of the supercurrent and voltage for decreasing (d) and increasing (i) current directions. (b) Suppercurrent current and voltage temporal dependence for the pair (I_3^d, I_3^i). The simulation parameters are same as for Fig. 2(b).

enough like in the left side of the step. This feature and its dependence on the model parameters will be investigated in detail somewhere else. The transition between the two states $m_y^{\pm}$ at $I = 0.45380$ for decreasing current is shown in Fig. 9(d) along with the moving average.

In Ref. [46,47] was noted that it is possible to apply microwave radiation with an ac magnetic field. If it is possible to weaken the electric field for the external electromagnetic radiation, and varying the magnetic field applied in the plane of the junction [47]. In this case, one can to tune the values of A and h_R to observe the Buzdin step, and transition between the two states of m_y. Also, this transition is manifested in phase shift of π for the supercurrent and voltage for the chimera step (or the Buzdin step if we apply only magnetic field).

VII. PHASE SHIFT ON THE CHIMERA STEP

An additional interesting property of the investigated system follows from the analysis of the temporal dependence of superconducting current and voltage at different points along the chimera step shown in Fig. 2(b). We choose several points fixed by dashed lines in Fig. 10(a) that lie on different branches of $m_y^{\rm av}$ and designated as I_n.

In Fig. 10(b), we illustrate the temporal dependence of the suppercurrent and voltage for the pair (I_3^d, I_3^i). As shown in the figure, if the two points lie on two different bubbles, a phase shift $(P_s) \approx \pi$ appears between them. This is confirmed by the negative value of Pearson correlation (PC) (see Sec. C in Ref. [44]). The results of our analysis for all points shown Fig. 10(a) are summarized in Table I where the P_s and PC are presented. The phase shift and Pearsons correlation takes intermediate values between the points at the same current direction (see Sec. D of Ref. [44]). This case is similar to the trivial SIS Josephson junction.

To understand the origin of the phase shifts which are demonstrated in Table I, let us consider the difference between the suppercurrent at two points on the step is given by $\delta I_s = \sin(\varphi_1 - r m_{y_1}) - \sin(\varphi_2 - r m_{y_2})$. In general, $\varphi_1 \neq \varphi_2$

TABLE I. Measurements of the phase shift (P_s) in degree and Pearsons correlation (PC) for several points shown in Fig. 2(b). Points $I_1^{d(i)}$ corresponds to $I = 0.4928$, $I_2^{d(i)}$ corresponds to $I = 0.4923$, $I_3^{d(i)}$ corresponds to $I = 0.4915$, $I_4^{d(i)}$ corresponds to $I = 0.4905$ and $I_5^{d(i)}$ corresponds to $I = 0.49$. We use (d) and (i) for decreasing and increasing current direction.

Pair	$I_s(t)$		V(t)	
	P_s	PC	P_s	PC
I_1^d, I_1^i	0°	1	0°	1
$I_1^{i(d)}, I_2^i$	176°	−0.888	179°	−0.898
I_3^d, I_3^i	177°	−0.932	181°	−0.931
$I_4^d, I_5^{i(d)}$	175°	−0.872	179°	−0.876
I_5^d, I_5^i	0°	1	0°	1

on the step, because the phase may take any value, however $d\varphi/dt =$ must be constant. Now, if $h_R = 0$, $G = 0$ and $r = 0$, the IV curve will demonstrate only Shapiro step (as in a single JJ). In this case, the suppercurrent will not show any phase shift by switching current direction at fixed current value. However, a phase shift appears if we sweep the current along the Shapiro step. In chimera step the situation is very interesting. A phase shift of 180° appears by switching the current direction due to the appearance of the two states of $m_y^{\pm}$ [i.e., if $m_y^{\text{av}}(I)$ changes sign]. Then the suppercurrent for the two points become out of phase, which is the case for two points on different bubble.

So, by switching the current direction (or apply current pulse), our results can provide an experimental way to observe the two states of magnetic moment and measure its hysteresis area by recording the suppercurrent (voltage) temporal dependence on each current step and then calculate the phase shift for both direction of current.

VIII. CONCLUSIONS

The interaction of the magnetic field of microwave radiation with the magnetic moment of the φ_0 Josephson junction leads to a number of unique resonant and synchronization phenomena. Particularly, due to the coupling of superconductivity and magnetism in this system, two mechanisms of synchronization of Josephson oscillations and magnetic precession appeared. The precession of the magnetic moment of the ferromagnetic layer, caused by the magnetic component of the external radiation, leads to the creation of the Buzdin and chimera steps in the I-V characteristics of the φ_0 junction [40].

We have explained the origin of bubble structure in the bias current dependence of magnetization in SFS φ_0 Josephson junction under external electromagnetic radiation. The appearance of two different dynamical states in the synchronization region chimera step of magnetic precession and Josephson oscillations on the I-V characteristics were demonstrated. These states are differed by the temporal dependence of the magnetic moment, and a phase shift of π appears in the suppercurrent and voltage dynamics. Moreover, the transition between these states leads to novel type of hysteresis which is strongly depend on the spin-orbit coupling and radiation parameters. We have demonstrated that the transition and hysteresis between theses locking states are reflected on the bifurcation diagram and I-V characteristics, so, the obtained results might be tested experimentally.

The existence of nonvanishing Josephson supercurrent in chimera and Buzdin steps, which appear in the dissipative state, allows the use of such junction in single-flux-quantum circuits [48–54] and Josephson voltage standards for metrology [54–57]. Also, the width of the Buzdin steps which has maximum values near FMR can be used as a probe for measuring the resonance frequency in φ_0 junctions. Because we observed the two dynamical states with phase shift of π at the same current value, their reflection on chimera and Buzdin steps can be used as a fingerprint for the detection of such type of φ_0 junction experimentally. We assume that our results might open the way to arrange a memory cell based on φ_0 junction, in which the reading can be done by measuring phase shift of voltage, and writing can be done by applying the current pulse. We consider that the appearance of phase shift in the voltage and suppercurrent signals may help to fabricate phase shifter devices based on φ_0 junctions.

ACKNOWLEDGMENTS

The authors are grateful to A. Buzdin, Y. Fominov, J. Tekic, I. R. Rahmonov, K. Kulikov, T. Belgibaev, G. Ovsyannikov, and K. Constantinian for fruitful discussion of some results of this paper. The work was carried out with the financial support of Project No. 24-21-00340 of Russian Science Foundation (RSF). Y.M.S. and M.N. acknowledge the financial support from collaborative project ASRT, Egypt – JINR, Russia. Special thanks to Cairo university, Alexandria library (Egypt), BLTP and the heterogeneous computing platform HybriLIT, LIT, JINR, Russia for the HPC servers.

[1] J. Linder and J. Robinson, Superconducting spintronics, Nat. Phys. **11**, 307 (2015).

[2] K.-R. Jeon, C. Ciccarelli, H. Kurebayashi, L. F. Cohen, X. Montiel, M. Eschrig, T. Wagner, S. Komori, A. Srivastava, J. W. A. Robinson, and M. G. Blamire, Effect of Meissner screening and trapped magnetic flux on magnetization dynamics in thick $Nb/Ni_{80}Fe_{20}/Nb$ trilayers, Phys. Rev. Appl. **11**, 014061 (2019).

[3] Yu. M. Shukrinov, Anomalous Josephson effect, Phys. Usp. **65**, 317 (2022).

[4] A. S. Mel'nikov, S. V. Mironov, A. V. Samokhvalov, A. I. Buzdin, Superconducting spintronics: State of the art and prospects, UFN **192**, 1339 (2022); Phys. Usp. **65**, 1248 (2022).

[5] I. A. Golovchanskiy, N. N. Abramov, V. S. Stolyarov, V. I. Chichkov, M. Silaev, I. V. Shchetinin, A. A. Golubov, V. V. Ryazanov, A. V. Ustinov, and M. Y. Kupriyanov,

Magnetization dynamics in proximity-coupled superconductor-ferromagnetsuperconductor multilayers, Phys. Rev. Appl. **14**, 024086 (2020).

[6] I. A. Golovchanskiy, N. N. Abramov, O. V. Emelyanova, I. V. Shchetinin, V. V. Ryazanov, A. A. Golubov, and V. S. Stolyarov, Magnetization dynamics in proximity-coupled superconductor-ferromagnet-superconductor multilayers. II. Thickness dependence of the superconducting torque, Phys. Rev. Appl. **19**, 034025 (2023).

[7] A. Buzdin, Direct coupling between magnetism and superconducting current in the Josephson φ_0 junction, Phys. Rev. Lett. **101**, 107005 (2008).

[8] F. Konschelle and A. Buzdin, Magnetic moment manipulation by a Josephson current, Phys. Rev. Lett. **102**, 017001 (2009).

[9] Y. Tanaka, T. Yokoyama, and N. Nagaosa, Manipulation of the Majorana fermion, andreev reflection, and Josephson current on topological insulators, Phys. Rev. Lett. **103**, 107002 (2009).

[10] J. Linder, Y. Tanaka, T. Yokoyama, A. Sudbø, and N. Nagaosa, Interplay between superconductivity and ferromagnetism on a topological insulator, Phys. Rev. B **81**, 184525 (2010).

[11] B. Lu, K. Yada, A. A. Golubov, and Y. Tanaka, Anomalous Josephson efect in *d*-wave superconductor junctions on a topological insulator surface, Phys. Rev. B **92**, 100503(R) (2015).

[12] F. Dolcini, M. Houzet, and J. S. Meyer, Anomalous Josephson effect in *d*-wave superconductor junctions on a topological insulator surface, Phys. Rev. B **92**, 035428 (2015).

[13] A. Zyuzin, M. Alidoust, and D. Loss, Josephson junction through a disordered topological insulator with helical magnetization, Phys. Rev. B **93**, 214502 (2016).

[14] J. Hasan, K. N. Nesterov, S. Li, M. Houzet, J. S. Meyer, and A. Levchenko, Anomalous Josephson effect in planar noncentrosymmetric superconducting devices, Phys. Rev. B **106**, 214518 (2022).

[15] W. Mayer, M. C. Dartiailh, J. Yuan, K. S. Wickramasinghe, E. Rossi, and J. Shabani, Gate controlled anomalous phase shift in Al/InAs Josephson junctions, Nat. Commun. **11**, 212 (2020).

[16] D. B. Szombati, S. Nadj-Perge, D. Car, S. R. Plissard, E. P. A. M. Bakkers, and L. P. Kouwenhoven, Josephson φ_0-junction in nanowire quantum dots, Nat. Phys. **12**, 568 (2016).

[17] A. Assouline, C. Feuillet-Palma, N. Bergeal, T. Zhang, A. Mottaghizadeh, A. Zimmers, E. Lhuillier, M. Eddrie, P. Atkinson, M. Aprili, and H. Aubin, Spin-orbit induced phase-shift in Bi_2Se_3 Josephson junctions, Nat. Commun. **10**, 126 (2019).

[18] A. Murani, A. Kasumov, S. Sengupta, Y. A. Kasumov, V. T. Volkov, I. I. Khodos, F. Brisset, R. Delagrange, A. Chepelianskii, R. Deblock, H. Bouchiat, and S. Guéron, Ballistic edge states in Bismuth nanowires revealed by SQUID interferometry, Nat. Commun. **8**, 15941 (2017).

[19] I. B. Bobkova, A. M. Bobkov, and M. A. Silaev, Magnetoelectric effects in Josephson junctions, J. Phys.: Condens. Matter **34**, 353001 (2022).

[20] D. S. Rabinovich, I. V. Bobkova, A. M. Bobkov, and M. A. Silaev, Resistive state of superconductor-ferromagnet-superconductor Josephson junctions in the presence of moving domain walls, Phys. Rev. Lett. **123**, 207001 (2019).

[21] M. Nashaat, I. V. Bobkova, A. M. Bobkov, Y. M. Shukrinov, I. R. Rahmonov, and K. Sengupta, Electrical control of magnetization in superconductor/ferromagnet/superconductor junctions on a three-dimensional topological insulator, Phys. Rev. B **100**, 054506 (2019).

[22] C. Guarcello and F. S. Bergeret, Cryogenic memory element based on an anomalous Josephson junction, Phys. Rev. Appl. **13**, 034012 (2020).

[23] G. A. Bobkov, I. V. Bobkova, and A. M. Bobkov, Controllable magnetic states in chains of coupled φ_0-Josephson junctions with ferromagnetic weak links, Phys. Rev. B **109**, 054523 (2024).

[24] Yu. M. Shukrinov, I. R. Rahmonov, K. Sengupta, and A. Buzdin, Magnetization reversal by superconducting current in φ_0 Josephson junctions, Appl. Phys. Lett. **110**, 182407 (2017).

[25] I. V. Bobkova, A. M. Bobkov, I. R. Rahmonov, A. A. Mazanik, K. Sengupta, and Yu. M. Shukrinov, Magnetization reversal in superconductor/insulating ferromagnet/superconductor Josephson junctions on a three-dimensional topological insulator, Phys. Rev. B **102**, 134505 (2020).

[26] S. Pal and C. Benjamin, Quantized Josephson phase battery, Europhys. Lett. **126**, 57002 (2019).

[27] M. Trahms, L. Melischek, J. F. Steiner, B. Mahendru, I. Tamir, N. Bogdanoff, O. Peters, G. Reecht, C. B. Winkelmann, F. von Oppen, and K. J. Franke, Diode effect in Josephson junctions with a single magnetic atom, Nature (London) **615**, 628 (2023).

[28] H. Narita, J. Ishizuka, R. Kawarazaki, D. Kan, Y. Shiota, T. Moriyama, Y. Shimakawa, A. V. Ognev, A. S. Samardak, Y. Yanase, and T. Ono, Field-free superconducting diode effect in noncentrosymmetric superconductor/ferromagnet multilayers, Nat. Nanotechnol. **17**, 823 (2022).

[29] C. Guarcello, F. S. Bergeret, R. Citro, Switching current distributions in ferromagnetic anomalous Josephson junctions, Appl. Phys. Lett. **123**, 152602 (2023).

[30] Yu. M. Shukrinov, A. Mazanik, I. R. Rahmonov, A. E. Botha, and A. Buzdin, Re-orientation of the easy axis in φ_0-junction, Europhys. Lett. **122**, 37001 (2018).

[31] K. V. Kulikov, D. V. Anghel, A. T. Preda, M. Nashaat, M. Sameh, and Yu. M. Shukrinov, Kapitza pendulum effects in a Josephson junction coupled to a nanomagnet under external periodic drive, Phys. Rev. B **105**, 094421 (2022).

[32] Yu. M. Shukrinov, and M. Nashaat, JINR collaboration with scientific institutions of Egypt in the field of theoretical research of superconducting Josephson nanostructures, Phys. Part. Nuclei **54**, 298 (2023).

[33] A. Janalizadeh, I. R. Rahmonov, S. A. Abdelmoneim, Yu. M. Shukrinovand, M. R. Kolahchi, Nonlinear features of the superconductor–ferromagnet–superconductor φ_0 Josephson junction in the ferromagnetic resonance region, Beilstein J. Nanotechnol. **13**, 1155 (2022).

[34] A. A. Mazanik, A. E. Botha, I. R. Rahmonov, and Yu. M. Shukrinov, Hysteresis and chaos in anomalous Josephson junctions without capacitance, arXiv:2311.00597.

[35] A. E. Botha, Yu. M. Shukrinov, J. Tekić, and M. R. Kolahchi, Chaotic dynamics from coupled magnetic monodomain and Josephson current, Phys. Rev. E **107**, 024205 (2023).

[36] Yu. M. Shukrinov, I. R. Rahmonov, and K. Sengupta, Ferromagnetic resonance and magnetic precessions in φ_0 junctions, Phys. Rev. B **99**, 224513 (2019).

[37] M. A. Silaev, Anderson-higgs mass of magnons in superconductor/ferromagnet/superconductor systems, Phys. Rev. Appl. **18**, L061004 (2022).

[38] S. Matsuo, T. Imoto, T. Yokoyama, Y. Sato, T. Lindemann, S. Gronin, G. C. Gardner, M. J. Manfra, and S. Tarucha, Phase engineering of anomalous Josephson effect derived from Andreev molecules, Sci. Adv. **9**, eadj3698 (2023).

[39] S. A. Abdelmoneim, Yu. M. Shukrinov, K. V. Kulikov, H. ElSamman, and M. Nashaat, Locking of magnetization and Josephson oscillations at ferromagnetic resonance in a φ_0 junction under external radiation, Phys. Rev. B **106**, 014505 (2022).

[40] Yu. M. Shukrinov, E. Kovalenko, J. Tekić, K. Kulikov, and M. Nashaat, Buzdin, Shapiro, and chimera steps in φ_0 Josephson junctions, Phys. Rev. B **109**, 024511 (2024).

[41] L. D. Landau, E. M. Lifshits, and L. P. Pitaevskii, *Theory of the Condensed State*, Course of Theoretical Physics Vol. 9 (Butterworth Heinemann, Oxford, 1991).

[42] M. Tinkham, *Introduction to Superconductivity*, 2nd ed. (Courier Corporation, 1996).

[43] M. Nashaat, M. Sameh, A. E. Botha, K. V. Kulikov, and Yu. M. Shukrinov, Bifurcation structure and chaos in dynamics of nanomagnet coupled to Josephson junction, Chaos **32**, 093142 (2022).

[44] See Supplemental Material at http://link.aps.org/supplemental/10.1103/PhysRevB.110.024510 for demonstrate the bifurcation for the Shapiro and Buzdin steps separately, effect of parameters on switching between the two states of m_y components. In addition to this, we demonstrate statistical methods to find the phase shift in voltage and suppercurrent for several points along chimera step, which also includes Ref. [45].

[45] A. D. Poularikas, *Transforms and Applications Handbook* (CRC Press, Boca Raton, FL, 2018).

[46] S. Mai, E. Kandelaki, A. F. Volkov, and K. B. Efetov, Interaction of Josephson and magnetic oscillations in Josephson tunnel junctions with a ferromagnetic layer, Phys. Rev. B **84**, 144519 (2011).

[47] S. E. Barnes, M. Aprili, I. Petković, and S. Maekawa, Ferromagnetic resonance with a magnetic Josephson junction, Supercond. Sci. Technol. **24**, 024020 (2011).

[48] J. Koch, T. M. Yu, J. Gambetta, A. A. Houck, D. I. Schuster, J. Majer, A. Blais, M. H. Devoret, S. M. Girvin, and R. J. Schoelkopf, Charge-insensitive qubit design derived from the Cooper pair box, Phys. Rev. A **76**, 042319 (2007).

[49] C. Monroe and J. Kim, Scaling the ion trap quantum processor, Science **339**, 1164 (2013).

[50] T. Golod, R. A. Hovhannisyan, O. M. Kapran, V. V. Dremov, V. S. Stolyarov, and V. M. Krasnov, Reconfigurable Josephson phase shifter, Nano Lett. **21**, 5240 (2021).

[51] Y. Yao, R. Cai, S.-H. Yang, W. Xing, Y. Ma, M. Mori, Y. Ji, S. Maekawa, X.-C. Xie, and W. Han, Half-integer Shapiro steps in strong ferromagnetic Josephson junctions, Phys. Rev. B **104**, 104414 (2021).

[52] N. O. Birge and N. Satchell, Ferromagnetic materials for Josephson π junctions, APL Mater. **12**, 041105 (2024).

[53] D. Pham, F. Li, K. Oba, Y. Takeshita, M. Tanaka, T. Yamashita, and A. Fujimaki, NbN-based tunnel-type π-junctions for low-power half-flux-quantum circuits, Supercond. Sci. Technol. **37**, 055004 (2024).

[54] S. Kim, L. V. Abdurakhimov, D. Pham, W. Qiu, H. Terai, S. Ashhab, S. Saito, T. Yamashita, and K. Semba, Superconducting flux qubit operating at zero magnetic field, arXiv:2401.14597.

[55] B. Jeanneret and S. P. Benz, Application of the Josephson effect in electrical metrology, Eur. Phys. J. Spec. Top. **172**, 181 (2009).

[56] R. S. Shaikhaidarov, K. H. Kim, J. W. Dunstan, I. V. Antonov, S. Linzen, M. Ziegler, D. S. Golubev, V. N. Antonov, E. V. Il'ichev, and O. V. Astafiev, Quantized current steps due to the a.c. coherent quantum phase-slip effect, Nature (London) **608**, 45 (2022).

[57] N. Crescini, S. Cailleaux, W. Guichard, C. Naud, O. Buisson, K. W. Murch, and N. Roch, Evidence of dual Shapiro steps in a Josephson junction array, Nat. Phys. **19**, 851 (2023).